

Comparative Study of Depth-Image Matching with Steepest Descendent and Simulated Annealing Algorithms

Hiroshi Noborio, Shogo Yoshida, Kaoru Watanabe, Daiki Yano and Masanao Koeda

Department of Computer Science, Osaka Electro-Communication University, Shijo-Nawate, Japan

Keywords: Simulated Annealing, Steepest Descendent, Organ-following Algorithm, Depth-Depth Matching.

Abstract: We have been developing a depth-depth matching-based organ-following algorithm for use in surgical navigation. In this paper, we experimentally compare the steepest descendent and simulated annealing algorithms under depth-depth matching. Our experiment can be performed in a real-life situation like practical surgery as follows: the organ is artificially occluded by another object corresponding to a human body, and surgery is performed on a real surgical bed beside two shadow-less lamps. In this research, in addition to the algorithm comparison, we checked the effect of the placement of two infrared shielding filters, SL999 and TS6080S. Based on the results, we could determine that the simulated annealing algorithm using the filter TS6080S is the best.

1 INTRODUCTION

Many types of surgical navigation systems have been developed in commercial and research fields. Nearly all systems in the commercial field can be seen at the "Medical expo" website (<http://www.medicaexpo.com/>). Several surgical navigation systems have been investigated in the research field as well.

However, the intended targets of such systems are the brain (Ferrolí, 2013; Schulz, 2012) or the bone (Blakeney 2011; Schnurr 2011). In almost all navigation researches, the bone is completely fixed by plastic components and consequently is not deformed. In addition, the brain is almost entirely confined by the skull and is not deformable except when considering the well-known case of brain shift. Therefore, the shape, position, and orientation of the brain and its inner parts such as several kinds of tumours, blood vessels, and nerves are precisely calculated.

Therefore, conventional surgical navigations systems do not consider large rotations/translations or deformations in the targeted systems. For this reason, we focus on the organ-following algorithm that considers the deformation by using a liver with arteries, veins, portal veins, and tumor, or brain with a shift, and so on (Noborio, 2013; Noborio, 2016a; Noborio 2016b). We compared several kinds of depth

cameras such as RICOH SV-M-S1, SICK V3310, Microsoft Kinect v1 and v2, Intel RealSense, and Euclid to get the deformation (the surface depth image) of the liver and brain during a real-time surgery. In this paper, we focused on following a real organ and scalpel cavitron ultrasonic surgical aspirator (CUSA) by its virtual organ and scalpel CUSA after calibrating both coordinate systems. Our previous papers addressed this agenda realistically by attaching some cameras directly besides a surgical bed in a real surgical room with two shadow-less lamps covered by two types of infrared filters. In this paper, while maintaining this realistic set-up, we experimentally compare two types of search algorithms—steepest descendent and simulation annealing. In addition, during the comparison, we tested the effect of placing two infrared shielding filters SL999 and TS6080S around the two shadow-less lamps. The results showed that the combination of simulation annealing and the infrared filter TS6080S is the best for following a real liver by its virtual liver in a real surgical room with two shadow-less lamps.

In section 2, we describe the real and virtual livers used in our experiment, and then explain our key idea of depth-image matching. In section 3, we first show our surgical room for an obstructed liver, which is equipped with two shadow-less lamps. Then, we compare the steepest descendent and simulated

annealing algorithms. Finally, in section 4, we present some concluding remarks.

2 DEPTH-IMAGE MATCHING AND OVERLAPPING RATIO BETWEEN REAL AND VIRTUAL LIVERS

From 2014, we have been developing several kinds of organ-following algorithms based on the steepest descendent algorithm from a virtual world simulation (Noborio, 2014a) to a real world experiment (Noborio, 2015a). In addition, we tested these algorithms in an experimental room and an actual surgical room with zero, one, and two shadow-less lamps. Moreover, we checked the usefulness of placing infrared shielding filters, SL999 and TS6080S (Noborio, 2017), on the lamp. Then, we recently compared the classic steepest descendent algorithm and the new simulated annealing algorithm in an actual surgical room with two shadow-less lamps enclosed by one of the two infrared filters, SL999 and TS6080S.

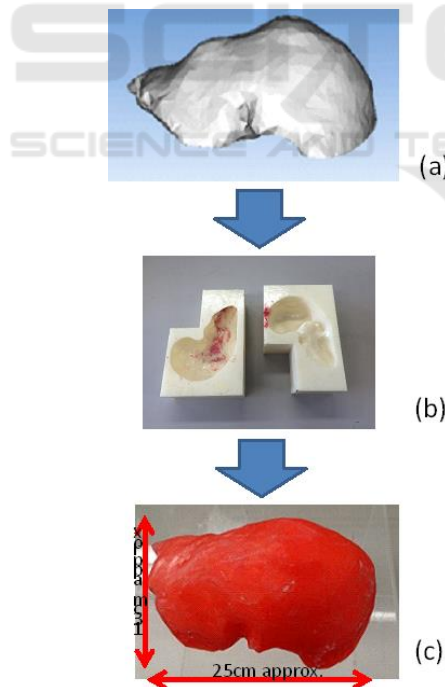


Figure 1: (a) Polyhedral liver in stereolithography STL format, (b) its 3D-printed plastic template, and (c) plastic liver pushed in the template.

In this chapter, we briefly explain our depth-depth matching method used in two kinds of search

algorithms. The function value generated by the depth-depth matching is used for the evaluation index of the search algorithm. Then, we explain in detail the steepest descendent and simulated annealing algorithms. The steepest descendent algorithm does not have a function for escaping from several local minima. Therefore, it sometimes overlooks the position/orientation where a virtual organ is coincident with the real organ. To overcome this, we prepared two kinds of randomized functions (Noborio, 2016c). Contrary to this, the simulated annealing algorithm includes the escaping function. Therefore, we do not need to prepare such a function additionally, which is an advantage.

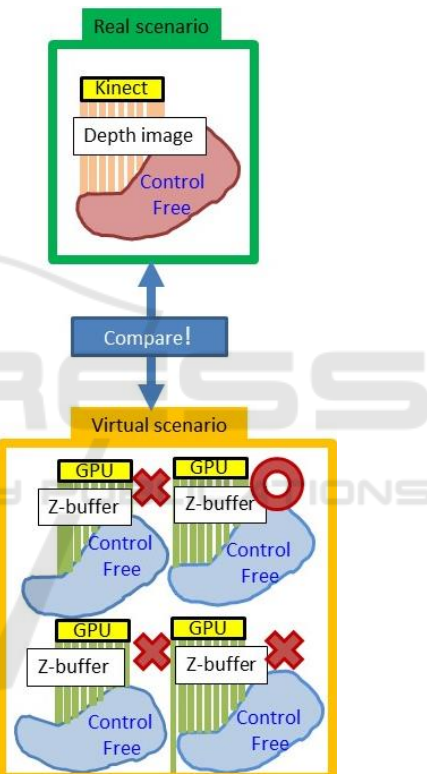


Figure 2: Position/orientation of the virtual liver model is analyzed to decrease the difference in its depth images and that of the actual liver.

2.1 Fast Depth-Depth Matching

The most important function in our surgical navigation is to track a virtual liver model (which is displayed to users) against a real liver, and to match the positions/orientations of the two liver samples at any time (Figure 1).

In our research, a depth camera such as the Kinect v2 captures the surface depth image of an organ. Simultaneously, the graphics processing unit (GPU)

board on the PC generates the surface depth image of the 3D virtual organ model. In Figure 2, we use the depth-image matching between the real and virtual worlds, whose positions and orientations were completely calibrated in advance.

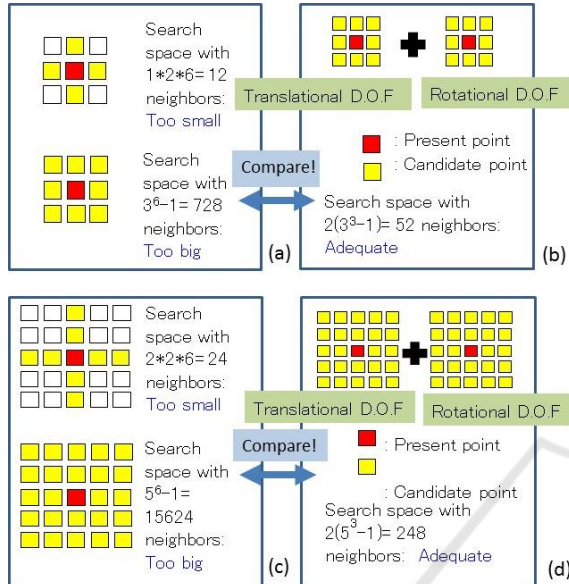


Figure 3: (a), (b) Search spaces containing 12 and 728 neighbouring candidates with six DOF space. (c),(d) Search spaces containing 52 and 248 neighbouring candidates with three translational DOF and three rotational DOF.

Each of the two kinds of proposed algorithms will always seek a better positon/orientation of the virtual liver against the positon/orientation of the real liver. By shifting slightly each time within the six degrees-of-freedom (DOF) space by $(x, y, z, \varphi, \theta, \psi)$, where x, y, z are the coordinates in the Euclidean 3D space, φ is the roll angle, θ is the pitch, and ψ is the yaw (Figure 3), we can find a better neighbouring point (positon/orientation) of the virtual liver whose overlapping ratio is minimum, as explained later. As mentioned in (Watanabe, 2015), searching the 6D digitalized space is quite time consuming. For this reason, we attempted to divide the 6D space into a 3D translation space and a 3D rotation space whose difference was changed from 1 to 3.

To obtain a function value (=overlapping ratio) using our search algorithm, it is better to match the real and virtual depth images for matching the real and virtual 3D point clouds (Liu, 2006; Wu, 2015). The reason is as follows:

- (1) The number of pixel depths is quite less than the number of points (Figure 4).
- (2) The former needs the sum of non-combinational distance differences (e.g., for 1024×1024 pixels)

but the latter requires the sum of combinatorial shortest distance calculations (e.g., for combination pairs between one million or more points in some point cloud) (Liu, 2006; Wu, 2015).

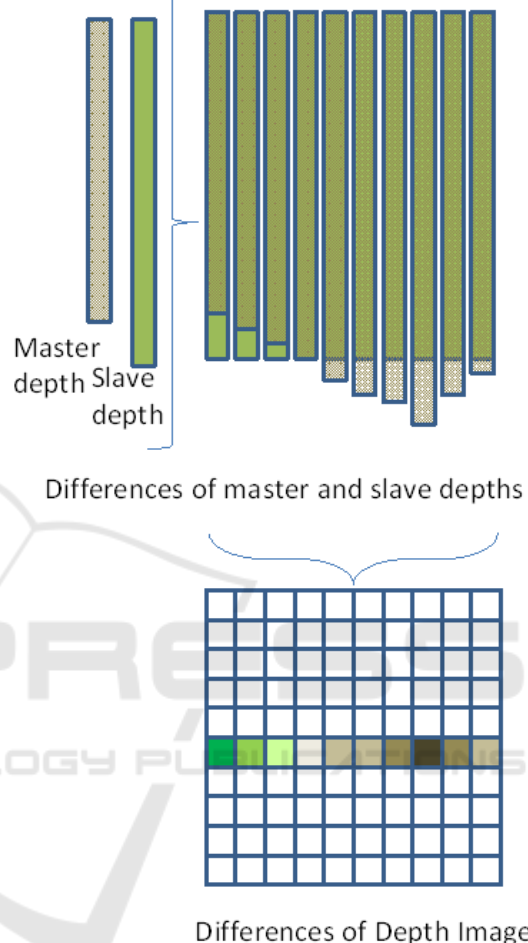


Figure 4: Summed differences between the real and virtual depth images based on pixels selected randomly in parallel on the GPU.

2.2 Randomized Algorithm based on Steepest Descendent

Using a selected search algorithm, we can match the positions and orientations of the virtual liver model and the real liver. As mentioned, we tested two kinds of randomized algorithms in order to decrease the differences between the depth images of the virtual and real liver models.

First, we designed a randomized algorithm based on steepest descendent (Figure 5), which is used in a real surgical room with an infrared filter, (Noborio, 2017) as follows:

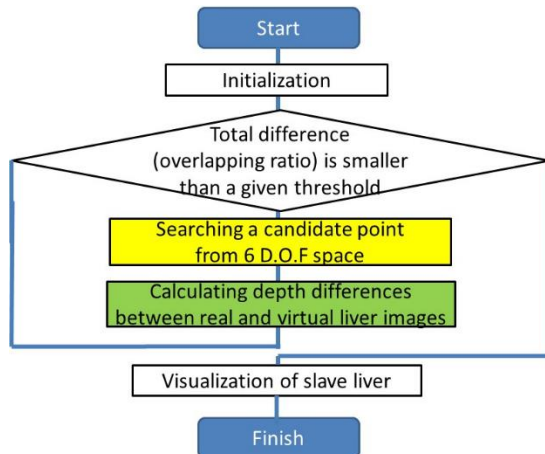


Figure 5: Flowchart illustrating depth-depth matching in our randomized algorithm, based on the steepest descendent method.

Given an initial guess x_0 , the method always computes a sequence of iterates x_k among six-dimensional digitalized space (three are the translational degrees-of-freedom and the other three are the rotational degrees-of-freedom).

At x_k , the algorithm always selects a neighbor whose randomized value f is minimized from many digitalized neighbors whose distances are 1 and 2 as x_{k+1} , as shown in Figure 3.

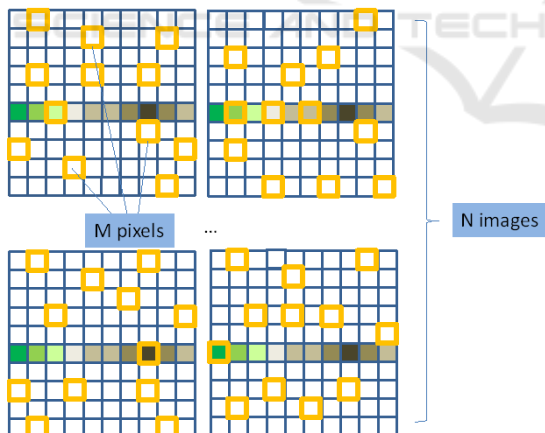


Figure 6: We randomly select a group of N pixels from each image. Then, we calculate the minimum, median, or average of the difference distribution between the real and virtual depth images. Furthermore, we select the minimum, median, or average of the evaluation values in M images. Their randomizations escape from a local minimum in the motion space in our steepest descendent.

In this algorithm, in order to escape from several local minima in the search space, we use two kinds of randomizations (Figure 6).

- (1) For each image, M pixels are randomly selected, and the minimum, median, or average of their differences are calculated.
- (2) For N images, we select their minimum, median, or average calculated in (1) as the evaluation value for the search.
- (3) In (1) and (2), we set M and N to 10, 50, and 100, respectively. This parameter selection is important for each organ.

2.3 Simulated Annealing Algorithm

In this section, we explain our simulated annealing algorithm as another type of randomized algorithm (Watanabe, 2017). Simulated annealing (SA) was first proposed in 1983 by Kirkpatrick et al. (Kirkpatrick, 1983). It was fortunately rediscovered in 1985 by Vlado Cerny (Cerny, 1985). SA is a metaheuristic that finds global optimization in a large search space. Steepest descent is a simple search method. At each step, it selects the best neighbor of the current point that is stuck at a local optimum and often cannot find a global optimum. SA selects a neighbor probabilistically and finds the global optimum for a sufficiently long time.

```

A_search(ti)
t ← ti
p ← position/orientation of the virtual liver
model at time ti
f ← fitness (p)
f_best ← f
p_best ← p
while (ti+1 − t > 0)
  randomly select a neighbor p' of p such
  that |p'i − pi| ≤ D for all i
  f' ← fitness(p')
  if f' < f_best then
    f_best ← f'
    p_best ← p'
  if f' < f   or
    random(0,1) ≥ (t − ti) / Δt then
    f_best ← f'
    p_best ← p'
  t ← t+1
  
```

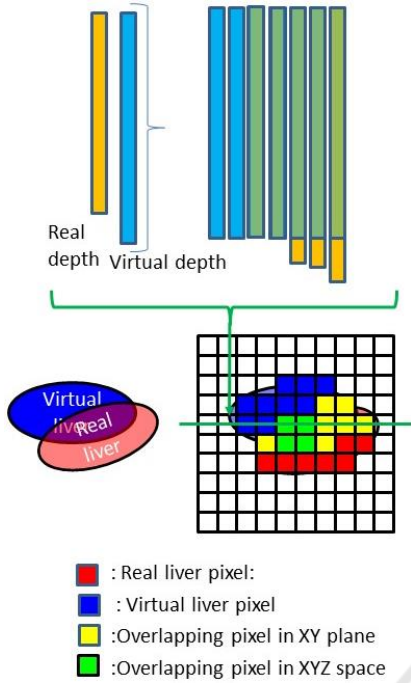


Figure 7: A 2D virtual liver, whose pixel is depicted in blue, is starting to overlap with its 2D real liver, whose pixel is depicted in red, in the depth image. In our matching system, the overlapping area in the XY plane is described by a set of yellow pixels, and the overlapping area in the XYZ space is described by a set of blue pixels.

The random function $(0,1)$ returns a random value from zero to one. The fitness (p') in this algorithm equals the randomized value f of the steepest descendent and it indicates the difference between the two depth images. The parameter D is half the width of the area, which is a six-dimensional hypercube with width $2D$, in which a new position/orientation p' is randomly generated. If D increases, the algorithm can choose a more distant neighbor to avoid falling into a local minimum.

In this algorithm, $f < f_{\text{best}}$ implies that we obtain the global minimum and $f < f$ implies that we obtain the local minimum. To escape from the local minimum, we prepare random $(0,1) \geq (t-t_i) / \Delta t$. Because Δt increases, the random value is selected to avoid falling into a local minimum. The camera can capture a part of the 3D liver through the circular hole.

First, we overlap a real liver by its virtual one in the 3D space by watching the pixel states generated by the real and virtual depth differences (Noborio 2015b). In our matching system (Figure 7), the areas projected from the real and virtual livers into the XY plane along the Z-axis are shown by sets of red and blue pixels, respectively. The pixel overlapped by real

and virtual livers in the XY plane is shown in yellow. Furthermore, the pixel overlapped by the real and virtual livers in the XYZ space is shown in blue. Therefore, an operator first moves the virtual liver in the horizontal XY space by eliminating the red and blue pixels in order to generate all yellow pixels. Then, we move the virtual liver in the vertical XYZ space by eliminating the yellow pixels and simultaneously generating blue pixels.

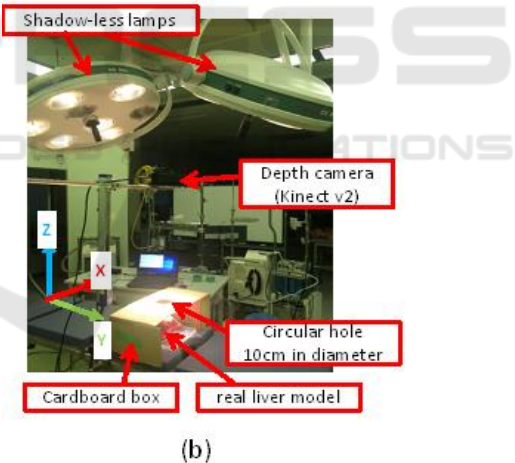
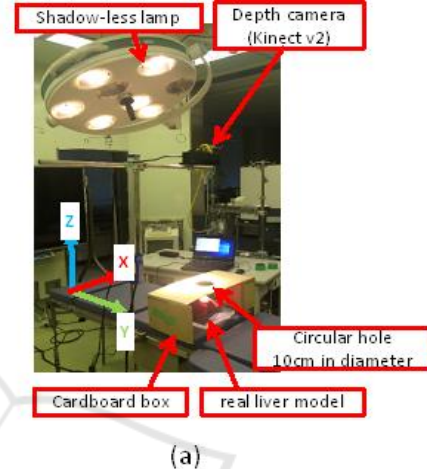


Figure 8: We compared two kinds of motion transcription algorithms in a real surgical room with (a) one shadow-less lamp (b) two shadow-less lamps covered by two kinds of invisible light filters. In our navigation, a 3D liver is always obstructed by a cardboard box with a circular hole.

3 COMPARATIVE EXPERIMENTAL RESULTS

In this chapter, we experimentally compared the steepest descendent and the simulated annealing algorithms with depth-depth matching.

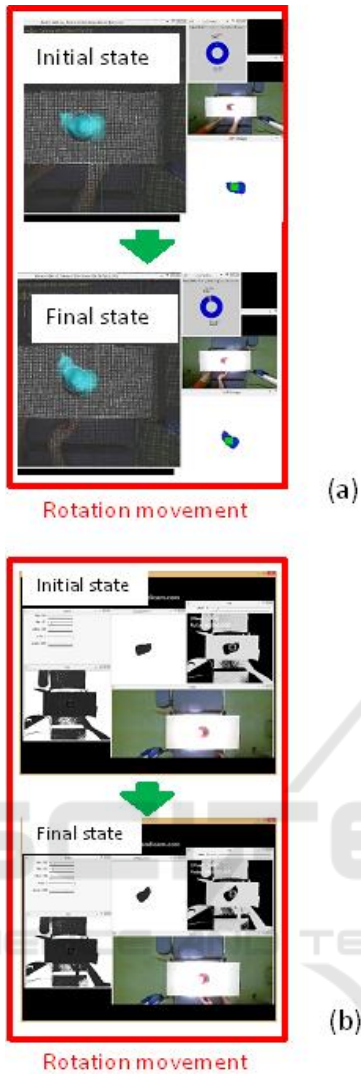


Figure 9: The same rotational movement is applied for the randomized steepest descendent (a) and simulated annealing algorithms (b). Unfortunately, right and left are opposite in all 2D RGB and depth images.

3.1 Experiments in a Real Surgical Room

In this section, we present several realistic experiments, which were conducted not in the laboratory, but in a surgical operating room. The experimental equipment is precisely described in Figure 8. An acrylic plate of length 25 cm, width of 25 cm, and thickness of 2 cm was placed on the operating table and a real liver was placed on the top of the plate. Consequently, an operator could flexibly move the liver. Movement of the liver was achieved by moving the acrylic plate instead of moving the actual liver itself.

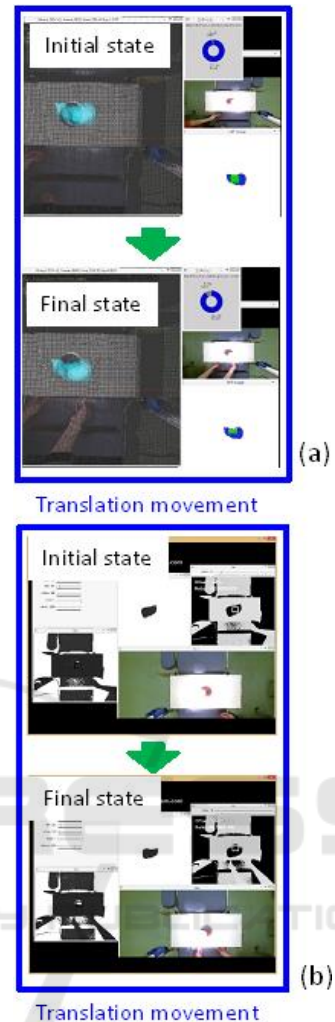


Figure 10: The same translational movement is applied for the randomized steepest descendent (a) and simulated annealing algorithms (b). Unfortunately, right and left are opposite in all 2D RGB and depth images.

Moreover, in order to conduct experiments involving occlusion, a cardboard sheet containing a hole of 10 cm in diameter was placed on the liver. The surface of this corrugated board was painted in light orange using a color spray to make it look like human skin. The camera (Kinect v2) was attached to a vertically movable robot. Therefore, it was able to change its distance from the liver according to different situations. The camera was placed horizontally with respect to the operating table at a height of 84 cm from the bottom of the actual liver. The camera system was fixed by attaching metal fittings to a metal rod. The metal rod was fixed to the camera, which was attached to the robot. The distance from the robot to the camera was set as 32 cm.

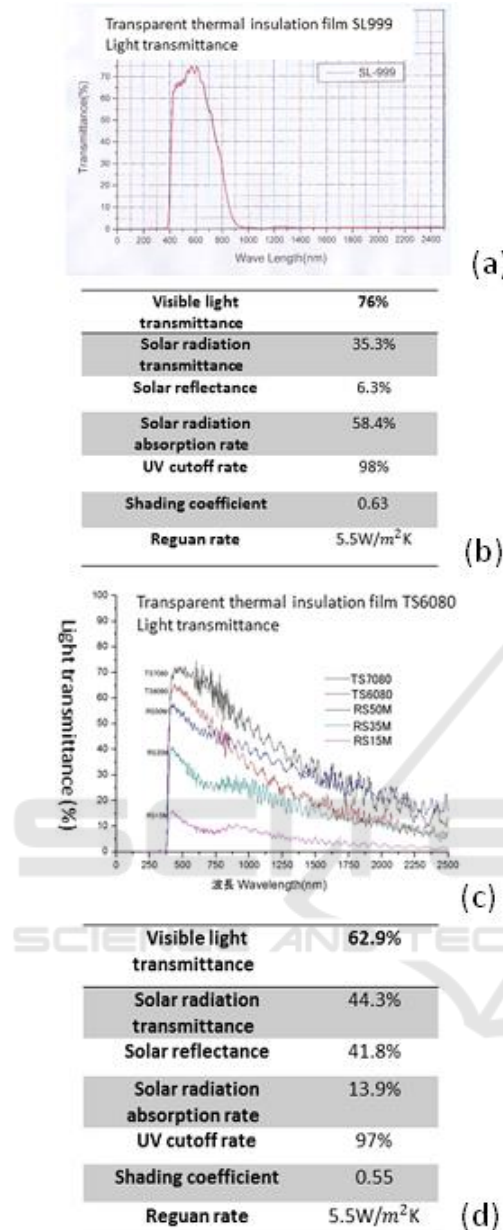


Figure 11: The light transmittance (a) and characteristics (b) of infrared shielding filter SL999, and the light transmittance (c) and characteristics (d) of infrared shielding filter TS6080.

The initial positions of the real liver and the virtual liver model were matched in the first experimental procedure. Next, the real liver placed on an acrylic board was covered with corrugated cardboard. It was subjected to rotational and translational movement within the corrugated cardboard box. It was done to ensure that the range of the liver visible from the hole of the cardboard did not

become less than half after the movement of the model. In our usual experiments, we select the offset value of 10 mm for real and virtual depth images against the 3D real liver and its polyhedron with the STL format in our surgical navigator. The model was rotated 45° around the center of the z-axis during the rotational movement (Figure 9), and it was moved by 5 cm in the y-axis direction during the parallel movement (Figure 10). Each co-ordinate axis is selected as shown in Figure 8.

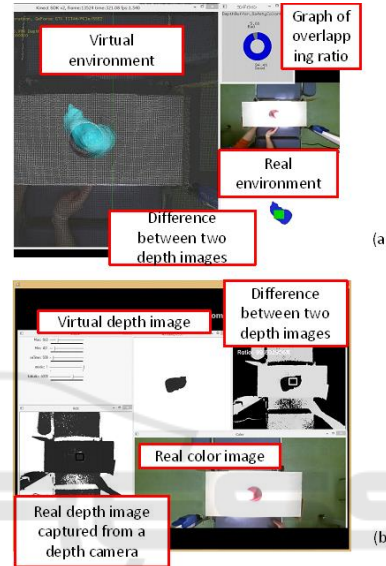


Figure 12: (a) Virtual and real RGB images, difference between the real and virtual depth images, and the graph of the overlapping ratio in the randomized steepest descendent algorithm, and (b) real RGB image and real and virtual depth images and their difference in the simulated annealing algorithm.

3.2 Comparison of Rotational Following Quality of the Two Algorithms

In this section, we compare the depth-depth matching-based organ-following algorithms for several surgical rotation operations. We use the steepest descendent (randomized) and simulated annealing algorithms as the organ-following scheme. Each algorithm always overlaps a virtual liver with its real liver. The quality of overlap is evaluated by the overlapping ratio explained in the previous section. It is individually checked for two lamps without any infrared shielding filter, with the SL999 or with the TS6080S (Figure 11).

The purpose behind using SL999 or TS6080S is that the depth camera itself uses infrared illumination.

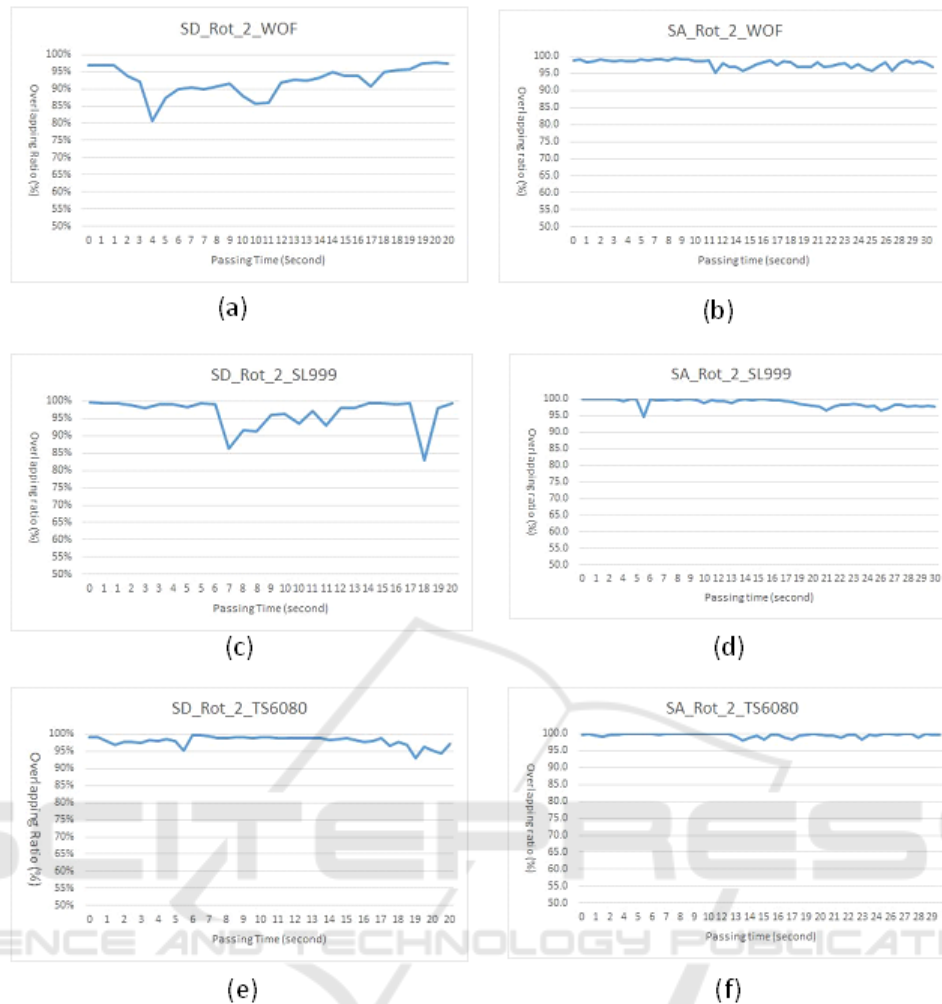


Figure 13: (a)(b) Comparative results of rotational liver operation between the randomized steepest descendent and simulated annealing algorithms under two shadow-less lamps without any infrared shielding filter. (c)(d) Comparative results of rotational liver operation between the randomized steepest descendent and simulated annealing algorithms under two shadow-less lamps with the infrared shielding filter SL999. (e)(f) Comparative results of rotational liver operation between the randomized steepest descendent and simulated annealing algorithms under two shadow-less lamps with the infrared shielding filter TS6080S.

Kinect v2 gets the depth images by the Time of Flight (TOF) method of projecting and receiving all infrared rays. Therefore, the camera strictly tries to gather the infrared rays of wavelength between 700 nm and 1000 nm. However, our shadow-less lamp projects the infrared rays of wavelength under 400 nm and over 1000 nm. Using our infrared filter SL999 or TS6080S, the ultra-violet light whose wavelength is between 10 nm and 400 nm is completely eliminated, but the visible light whose wavelength is between 400 nm and 700 nm is not eliminated. In addition to this, the infrared light and the radio waves over 1000 nm are partially passed.

In our navigation system, we prepared a different set of windows for the two algorithms, as described

in Figure 12. The reason is that the steepest descendent (randomized) algorithm was formulated during 2013–2015. In contrast, the simulated annealing algorithm was independently developed during 2016–2017.

However, in our navigation system, experimental data such as sequences of real RGB images and depth images during several kinds of surgical operations in a real surgical room were completely memorized in the PC under no infrared shielding filter. The reason is as follows: a surgical room is always used by many doctors, students, and researchers for surgeries, lectures, and researches. Therefore, our experimental data such as the sequences of lighting conditions during surgeries, which were obtained from the surgi-

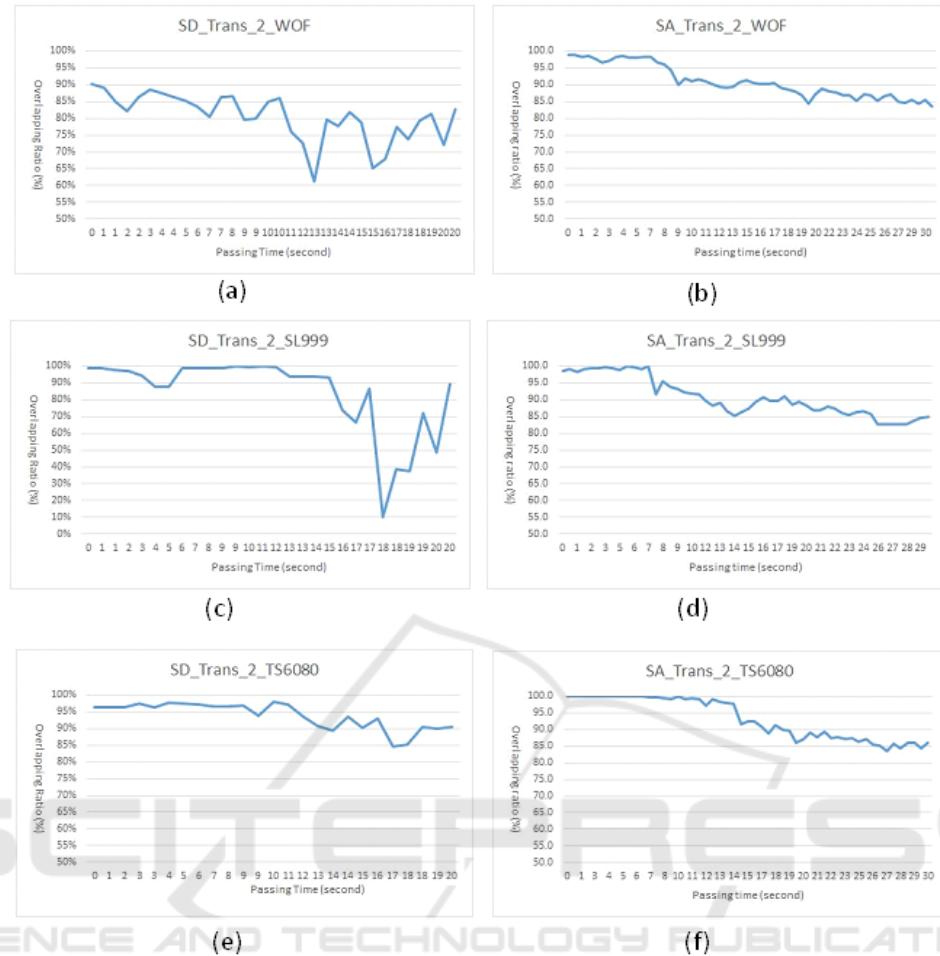


Figure 14: (a)(b) Comparative results of translational liver operation between the randomized steepest descendent and simulated annealing algorithms under two shadow-less lamps without any infrared shielding filter. (c)(d) Comparative results of translational liver operation between the randomized steepest descendent and simulated annealing algorithms under two shadow-less lamps with the infrared shielding filter SL999. (e)(f) Comparative results of translational liver operation between the randomized steepest descendent and simulated annealing algorithms under two shadow-less lamps with the infrared shielding filter TS6080S.

cal room, are quite valuable. For this reason, all the experimental information pertaining to the surgical room was completely memorized and the algorithm performance by varying several kinds of parameters was checked again against the experimental information in our laboratory. Therefore, we compared two or more types of algorithms for the same sequences of lighting.

A real liver is moved rotationally, and then its virtual liver model follows the real liver. The same rotational movement is used for the randomized steepest descendent and simulated annealing algorithms (Figure 9). As shown in Figure 13, the initial overlapping ratio is over 97% (nearly equals 100%). When moved rotationally, as illustrated in Figure 9, a variation in the overlapping ratio is

observed during the operation shown in Figure 13. In almost all cases, the overlapping ratio obtained in the simulated annealing algorithm was always better than that achieved in the randomized steepest descendent algorithm. Moreover, the overlapping ratio generated by two lamps with TS6080S was always better than with the other filter. As a result, the simulated annealing algorithm using the filter TS6080S is experimentally found to be the best with regard to the rotational operation in liver surgery.

3.3 Comparison of Translational Following Quality of the Two Algorithms

A real liver is moved translationally, and then its vir-

tual liver model follows the real liver. The same translational movement is applied to the randomized steepest descendent and simulated annealing algorithms (Figure 10).

As shown in Figure 14, each overlapping ratio is over 97% (nearly equals 100%). The variation in the overlapping ratio under translational movement (Figure 10) is shown in Figure 14. In almost all cases, the poorest overlapping ratio obtained in the simulated annealing algorithm is clearly better than that obtained in the randomized steepest descendent algorithm. Contrary to this, the overlapping ratios generated by two lamps without any filter are almost the same in the simulated annealing algorithm. As a result, with respect to the translational operation of liver surgery, the simulated annealing algorithm is better but using the filters is experimentally meaningless.

4 CONCLUSIONS

In this paper, we have given several comparative results of depth-depth-image matching-based organ-following algorithms. Compared with our previous laboratory experiments, or without the addition of a shadow-less lamp, this experiment can be applied to real-life situations such as practical surgery as follows: the organ is artificially occluded by another object, and the surgical operation is performed on a real surgical bed beside two shadow-less lamps. In this research, in addition to the comparison of two kinds of algorithms, we checked the usefulness of two infrared shielding filters, SL999 and TS6080S. Based on the results, we could determine that the simulated annealing algorithm using the filter TS6080S is the best.

At present, we are looking forward to using an infrared filter, which can pass light of wavelength between 700 nm and 1000 nm. In the near future, we will try to verify the rotational or translational following stability of our algorithm by using more effective infrared shielding filters.

ACKNOWLEDGEMENTS

This study was partly supported by the 2014 Grants-in-Aid for Scientific Research (No. 26289069) from the Ministry of Education, Culture, Sports, Science and Technology, Japan. The study was also supported by the 2014 Cooperation Research Fund from the

Graduate School at Osaka Electro-Communication University.

REFERENCES

- Ferroli, P., Tringali, G., Acerbi, F., Schiariti, M., Broggi, M., Aquino, D., Broggi, G., 2013. Advanced 3-dimensional planning in neurosurgery, *Neurosurg Suppl. 1*, pp.A54–A62. doi:10.1227/NEU.0b013e3182748ee8.
- Schulz, C., Waldeck, S., Mauer, M., 2012. Intraoperative image guidance in neurosurgery: development, current indications, and future trends, *Radiol Res Pract* 197364. doi:10.1155/2012/197364.
- Blakeney, G., Khan, J., Wall, J., 2011. Computer-assisted techniques versus conventional guides for component alignment in total knee arthroplasty: a randomized controlled trial, *J Bone Joint Surg Am.* 93, pp.1377–1384. doi: 10.2106/JBJS.I.01321.
- Schnurr, C., Eysel, P., König, P., 2011. Displays mounted on cutting blocks reduce the learning curve in navigated total knee arthroplasty, *Comput Aided Surg.* 16:249–256. doi: 10.3109/10929088.2011.603750.
- Noborio, H., et al., 2013. A Fast Surgical Algorithm Operating Polyhedrons Using Z-Buffer in GPU. In *9th Asian Conference on Computer Aided Surgery*, Waseda University, Tokyo Japan, pp.110-111.
- Noborio, H., et al., 2016a. Fast Surgical Algorithm for Cutting with Liver Standard Triangulation Language Format Using Z-Buffers in Graphics Processing Unit. Computer Aided Surgery, DOI:10.1007/978-4-431-55810-1, pp.127-140.
- Noborio, H., et al., 2016b. Depth Image Matching Algorithm for Deforming and Cutting a Virtual Liver via its Real Liver Captured by Kinect v2. In *IWBBI 2016*, LNBI 9656, pp.196-205, DOI: 10.1007/978-3-319-31744-1_18.
- Watanabe, K., et al., 2015. A New 2D Depth-Depth Matching Algorithm whose Translation and Rotation Freedoms are Separated. In *ICIIBMS2015, Track 3: Bioinformatics, Medical Imaging and Neuroscience*, OIST, Okinawa Japan, pp.271-278, 2015.
- Liu, Y., 2006. Automatic registration of overlapping 3D point clouds using closest points. *Journal of Image and Vision Computing*, Vol. 24, No. 7, pp.762-78.
- Wu, F., Wang, W., Lu, Q., Wei, D., Chen, C., 2015. A new method for registration of 3D point sets with low overlapping ratios. In *13th CIRP Conference on Computer Aided Tolerancing*, pp.202-206.
- Noborio, H., et al., 2016c. Tracking a Real Liver using a Virtual Liver and an Experimental Evaluation with Kinect v2. In *IWBBI 2016*, LNBI 9656, pp.149-162, DOI: 10.1007/978-3-319-31744-1_14.
- Noborio, H., et al. 2014. Motion Transcription Algorithm By Matching Corresponding Depth Image and Z-buffer, In *10th Anniversary Asian Conference on Computer Aided Surgery*, pp.60-61.

- Noborio, H., et al. 2015a. Experimental Results of 2D Depth-Depth Matching Algorithm Based on Depth Camera Kinect v1. *Journal of Bioinformatics and Neuroscience*, Vol.1, No.1, pp.38-44.
- Noborio, H., et al., 2017. Algorithm Experimental Evaluation for an Occluded Liver with/without Shadow-Less Lamps and Invisible Light Filter in a Surgical Room. In *HCI 19, Lecture Notes in Computer Science book series (LNCS, volume 10289)*, pp.524-539, DOI: 10.1007/978-3-319-58637-3_41.
- Watanabe, K., et al, 2017. A New Organ-Following Algorithm Based on Depth-Depth Matching and Simulated Annealing, and Its Experimental Evaluation. In *HCI 19, Lecture Notes in Computer Science book series (LNCS, volume 10289)*, DOI:10.1007/978-3-319-58637-3_47 pp.594-607.
- Kirkpatrick, S., Gelatt, D., Vecchi, P., 1983. Optimization by simulated annealing. *Science* 220 (4598), pp.671-680. DOI:10.1126/science.220.4598.671. JSTOR 1690046. PMID 17813860.
- Cerny, V., 1985. Thermodynamical approach to the traveling salesman problem: An efficient simulation algorithm. *Journal of Optimization Theory and Applications*, Vol.45, No.1, pp.41-51. DOI:10.1007/BF00940812.
- Noborio, H, et al. 2015b. Image-based Initial Position/Orientation Adjustment System between Real and Virtual Livers," *Jurnal Teknologi, Medical Engineering*, Vol. 77, No.6, pp. 41-45, DOI:10.11113/jt.v77.6225, Penerbit UTM Press, E-ISSN 2180-3722.